HHS Public Access

Author manuscript

*Acta Biomater*. Author manuscript; available in PMC 2019 March 01.

Published in final edited form as:

*Acta Biomater*. 2018 March 01; 68: 113–124. doi:10.1016/j.actbio.2017.12.023.

# Repurposing Disulfiram for Cancer Therapy via Targeted Nanotechnology through Enhanced Tumor Mass Penetration and Disassembly

**Huacheng He**, **Dr. Eleni Markoutsa**, **Jing Li**, and **Dr. Prof. Peisheng Xu***

Department of Drug Discovery and Biomedical Sciences, College of Pharmacy, University of South Carolina

## Abstract

Disulfiram (DSF), an FDA approved drug for the treatment of alcoholism, degrades to therapeutically active diethyldithiocarbamate (DDTC) in the body by reduction. Hereby, we developed a redox sensitive DDTC-polymer conjugate for targeted cancer therapy. It was found that the DDTC-polymer conjugate modified with a β-D-galactose receptor targeting ligand can self-assemble into LDNP nanoparticle and efficiently enter cancer cells by receptor-mediated endocytosis. Upon cellular uptake, the LDNP nanoparticle degrades and releases DDTC due to the cleavage of disulfide bonds, and subsequently forms copper (II) DDTC complex to kill a broad spectrum of cancer cells. 3D cell culture revealed that this nanoparticle shows much stronger tumor mass penetrating and destructive capacity. Furthermore, LDNP nanoparticles exhibited much greater potency in inhibiting tumor growth in a peritoneal metastatic ovarian tumor model.

### Keywords

repurpose; disulfiram; cancer; polymer-drug conjugate; nanoparticle

## 1. Introduction

Disulfiram (DSF) is an FDA approved drug that has been used for the treatment of alcoholism for over 60 years [1]. In the last decade, many studies demonstrated that DSF has great potential for cancer therapy [2–5]. It was revealed that DSF inhibits tumor growth, angiogenesis, invasion, and metastasis [6, 7]. In addition, studies found that DSF reduces drug resistance of cancer cells by suppressing P-glycoprotein (P-gp) transport activity [8–10]. Although the detailed anticancer mechanism of DSF is not fully understood, its cytotoxicity is believed to relate to the intracellular formation of metabolite-copper complexes. As a bivalent metal ion chelator, DSF can enter cancer cells, degrade to

715 Sumter St., Columbia, SC 29208, United States, xup@cop.sc.edu.

Supporting Information

Supporting Information is available from the Wiley Online Library or from the author.

diethyldithiocarbamate (DDTC) and intracellularly form a copper-DDTC complex ($Cu(DDTC)_2$) [4]. $Cu(DDTC)_2$ induces elevated reactive oxygen species (ROS) level, which exceeds the antioxidant capacity of cancer cells and subsequently results in the apoptosis of cancer cells [11]. $Cu(DDTC)_2$ may also regulate intracellular signaling [12, 13], enzyme activities [14] (such as acetaldehyde dehydrogenase (ALDH)) [15], and inhibit proteasome function [16]. Since many tumors have a higher copper concentration, up to 2–3 fold compared to normal tissues, the copper dependent anticancer activity of DSF makes it a great candidate for cancer therapy [17]. Therefore, the application of DSF may selectively kill cancer cells while sparing normal cells.

Although the combination of DSF and copper gluconate for cancer treatment has been adopted in many ongoing clinical trials, the systemic application of DSF is limited due to its hydrophobicity. Besides that, DSF is easily metabolized into less effective molecules in the blood stream and in an acidic gastric environment, resulting in an inadequate DSF concentration at tumor sites [18]. As a consequence, DSF can only kill a fraction of cancer cells, which probably is the main cause for the failure of several clinical trials involved with DSF. To address these issues, several DSF loaded nanoparticles have been developed to deliver DSF to tumor sites [19–22]. Nanoparticles can improve DSF solubility, isolate it from labile environment and enhance its accumulation in the tumor tissue, which altogether result in a better anticancer efficacy. Currently reported DSF delivery systems mainly focused on physical encapsulation of DSF in nanostructures [23, 24]. Due to the nature of these nanoparticles, unwanted premature drug release is unavoidable, which may still diminish the anticancer efficacy of DSF. Therefore, developing a safe and effective DSF delivery system for in vivo application becomes extremely important.

Our previous research developed a polymer called poly[(2-(pyridin-2-yldisulfanyl) ethyl acrylate)-co-[poly(ethylene glycol)]] (PDA-PEG) [25–27], which contains multiple pyridine-2-thiol groups. Due to the nature of pyridine-2-thiol, PDA-PEG can be easily modified by various thiol-containing molecules through thiol-disulfide exchange reaction to form polymer-drug conjugates. Through this approach, premature drug release during circulation can be prohibited. Upon cellular uptake, with the help of intracellular high GSH concentration, the drug could be rapidly released after the cleavage of disulfide bonds to exhibit its therapeutic effect [26].

Gunn et al. explored D-galactose receptor expression in various ovarian cancer cell lines, including SHIN3 SKOV-3,CaOV3, and A2780, and found all these cell lines were expressing D-galactose receptor, through which cellular uptake of -conjugated serum albumin was enhanced [28], suggestion D-galactose receptor is a great marker for ovarian cancer targeted drug delivery. Recent study found that lactobionic acid (LBA) is a selective ligand for D-galactose receptor and proved effective in targeting cancer cells [29].

Thus, we aimed to develop a LBA functionalized polymer-drug conjugate for the delivery of DSF based on the excellent intracellular releasing property of PDA-PEG based carrier. Since the main metabolite of DSF is DDTC, which is the therapeutically active compound for DSF in killing cancer cells, we propose to repurpose DSF by developing a DDTC-polymer conjugate for tumor targeted DSF delivery (Scheme 1).

## 2. Materials and Methods

### 2.1. Chemicals

Aldrithiol-2 and Silica gel (Spherical, 100 mm) were purchased from Tokyo Chemical Industry Co., LTD (Harborgate Street, Portland, OR). 2-Mercaptoethenol, DL-dithiothreitol (DTT), tris(2-carboxyethyl)phosphine (TCEP), 2, 2-Azobisisobutyronitrile (AIBN), (3-(4,5-dimethylthiazol-2-yl)-2,5-diphenyltetrazolium bromide (MTT), Poly(ethylene glycol) methacrylate (Mn=360 Da), sodium diethyldithiocarbamate (DDTC) were purchased from Sigma Aldrich Chemical Co. (St. Louis, MO). Penicillin (10,000 U/mL), streptomycin (10,000 mg/mL), 0.25% trypsin-EDTA, Dulbecco's Modified Eagle Medium (with L-glutamine) and fetal bovine serum (FBS) were obtained from American Type Culture Collection (ATCC, Manassas, VA). Cy3-NHS was purchased from Lumiprobe Corporation (Hallandale Beach, FL). D-luciferin was purchased from PerkinElmer Inc. All the other solvents used in this research were purchased from Sigma Aldrich Chemical Co. (St. Louis, MO) and used without further purification unless otherwise noted.

### 2.2. Cell culture

SKOV-3 ovarian cancer cells, TiB-73 normal liver cells, HepG2 liver cancer cells, HCT-116 colon cancer cells, MDA-MB-231 breast cancer cells, SKBR3 breast cancer cells, and NCI-Adr-Res drug resistant ovarian cancer cells were purchased from ATCC. Cells were cultured at 37 °C under 5% $CO_2$ in phenol red-containing Dulbecco's modified Eagle medium (DMEM; Gibco Life Tech., cat. #11960-044) supplemented with 10% heat-inactivated fetal bovine serum (Omega scientific, cat. #FB02) and the antibiotics penicillin/streptomycin (Corning Cellgro, cat. #30-002-C1). Cells were sub-cultured in T-75 flasks at 70–80% confluency every 2–3 days.

### 2.3. PDA-PEG synthesis

PDA-PEG polymer was synthesized according to our previous reports. Briefly, PDA (241.3 mg (1 mmol) and PEG360 (1 mmol, 360 mg) were dissolved in 5 mL degassed anisole. 2,2-Azobisisobutyronitrile (AIBN, 14 mg (0.085 mmol) in 1 mL degassed anisole was then added, and the reaction mixture was stirred for 24 h at 65 °C. The final product was precipitated (3×) in ice cold ether and dried for 48 h in vacuum. The structure of PDA-PEG was confirmed by $^{1}$H-NMR, and its molecular weight and polydispersity were evaluated by gel permeation chromatography (GPC).

### 2.4. PDA-PEG-DSF and LBA-PDA-PEG-DSF synthesis

PDA-PEG was further modified by lactobionic acid (LBA) and diethyldithiocarbamate (DDTC) to yield PDA-PEG-DSF (Scheme 2). Briefly, PDA-PEG (20 mg in 500 μL DMSO) was firstly mixed with cysteamine (0.56 mg in 500 μL DMSO, 20% PDA function group) and reacted overnight at room temperature. After that, LBA (4.33 mg in 100 μL DMSO) was activated by 1-Ethyl-3-[3-dimethylaminopropyl]carbodiimide hydrochloride (EDC, 4.64 mg in 100 μL DMSO) and N-hydroxysuccinimide (NHS, 2.79 mg 100 μL DMSO) for 30 min and added to the polymer solution. After overnight reaction at room temperature, Sodium diethyldithiocarbamate (DDTC (2.76 mg in 100 μL DMSO) was added with 10 μL acetic

acid and left for 24 h. The final solution was dialyzed towards DMSO (MW CO=1,000 Da) to remove unreacted LBA and DDTC and precipitated in cold ether and dried in a vacuum oven to obtain the LBA-PDA-PEG-DSF. For PDA-PEG-DSF, unmodified PDA-PEG was mixed with DDTC and all other conditions were the same as the synthesis of LBA-PDA-PEG-DSF. The structure of PDA-PEG-DSF and LBA-PDA-PEG-DSF was confirmed by $^{1}$H-NMR.

### 2.5. LBA-PDA-PEG-DSF-Cy3 synthesis

PDA-PEG-DSF was modified by Cy3 for cellular uptake study. Briefly, cysteamine (0.84 mg, 30% PDA function group) in 500 μL DMSO was added dropwise into 20 mg PDA-PEG in 500 μL DSMO and the reaction mixture was left at room temperature overnight. After overnight reaction, Cy3 NHS ester (0.142 mg in 20 μL DMSO, 5% PDA function group) was added and the mixture was left for reaction for 2 h at room temperature. For LBA conjugation, LBA (4.33 mg in 100 μL DMSO) was activated by EDC (4.64 mg in 100 μL DMSO) and NHS (2.79 mg 100 μL DMSO) for 30 min and added to the polymer solution and reacted overnight. Both PDA-PEG-Cy3 and LBA-PDA-PEG-Cy3 then reacted with DDTC to get Cy3 labeled polymers (PDA-PEG-Cy3-DSF and LBA-PDA-PEG-Cy3-DSF). The reaction mixture was finally followed with a thorough dialysis towards DMSO to remove free Cy3 and DDTC. The concentration of Cy3 in the final product was measured by microplate reader (Ex=485 nm, Em= 595nm, Beckman Coulter DTX 880 Multimode Detector, Beckman Coulter, Inc).

### 2.6. DDTC quantification by HPLC

DSF concentration in polymers was quantified by HPLC. In brief, PDA-PEG-DSF or LBA-PDA-PEG-DSF was firstly dissolved in PBS (0.5 mg polymer /mL). After that, 100 mM DTT was added and incubated for 1 h to release DDTC from the polymer. The final polymer concentration was 0.25 mg/mL. DDTC concentration was finally quantified by HPLC (methanol:$H_2O$ (0.1% formic acid)=65:35 at 214 nm, flow rate=0.6 mL/min).

### 2.7. Dynamic light scattering (DLS) and Transmission electron microscopy (TEM)

The size and morphology of the polymer in water were monitored by DLS and TEM. For DLS, PDA-PEG-DSF and LBA-PDA-PEG-DSF were dissolved in dd$H_2O$ (1 mg/mL) with or without 10 μM $CuCl_2$ and the sizes were recorded by Zetasizer (Malvern Instruments Ltd). For TEM, PDA-PEG-DSF (1 mg/mL in ddH2O with or without 10 μM $CuCl_2$) was dropped onto copper grids and air dried prior to image.

### 2.8. DDTC release from PDA-PEG-DSF nanoparticle

Nanoparticles (0.25 mg/mL) were suspended in PBS buffer (pH7.4, 10 mM) with or without 10 mM GSH and immediately loaded to HPLC and injected every 20 min. DSF released from polymer was then calculated referred to a pre-established calibration curve.

### 2.9. Cellular uptake observed by confocal microscopy

SKOV-3 (200,000 cells/dish) was seeded in 35 mm Petri dishes (Mat Tek, MA, USA) overnight. PDA-PEG-Cy3-DSF and LBA-PDA-PEG-Cy3-DSF diluted in culture medium

were then added (equivalent to 0.1 μg/mL Cy3). To block the asialoglycoprotein receptor (ASGP-R), free LBA (final concentration 1 mg/mL) was added to the dishes with LBA-PDA-PEG-Cy3-DSF. After 3 h incubation under a humidified atmosphere of 95/5% air/$CO_2$, cells were washed by PBS (3×), fixed with formaldehyde (4.5% in PBS) and stained with Hoechst 33342 (final concentration 1μg/mL). Then cells were analyzed under a confocal microscope (LSM 700, Carl-Zeiss Inc.).

### 2.10. Flow cytometry

SKOV-3 (300,000cells/well) was seeded in 6-well plate overnight. PDA-PEG-Cy3-DSF, LBA-PDA-PEG-Cy3-DSF and LBA-PDA-PEG-Cy3-DSF with free LBA (1 mg/mL) were added and incubated for 3 h under a humidified atmosphere of 95/5% air/$CO_2$. Then cells were washed, trypsinized, and resuspened in PBS. Cy3 positive cell population was quantified at $\lambda_{ex}$488 and $\lambda_{em}$585 nm using flow cytometry (BD Accuri C6, BD Biosciences).

**MTT assay—**In vitro cytotoxicity of DNP and LDNP was tested in cancer cell lines, including MDA-MB-231, SKOV-3, NCI/ADR-Res, HCT 116, SKBR3, and HepG2, and TiB-73 normal liver cell line. Cells were seeded in 96-well plate (20,000 cells/well) for 24 h prior to the study. Then a series of concentrations of disulfiram (DSF), DNP, LDNP in culture medium were added, supplementing with or without $CuCl_2$ (10 μM). The cells were then incubated 24 h in in 95/5% air/$CO_2$ at 37 °C. After 24 h, MTT reagent (100 μL, 10% (w/w) in medium) was added and incubated for 4 h, following the addition of MTT stop solution and the measurement of the optical density of the medium using a microplate reader (ELX808, Bio-Tech Instrument, Inc) at λ = 595 nm.

### 2.11. Tumor Spheroid

**a) Uptake of LBA-PDA-PEG-Cy3-DSF—**SKOV-3 cells were seeded in Corning® Ultra-Low Attachment 96-well plate (20,000 cells/well). After 24 h, each well formed one tumor spheroid. After 5 days, PDA-PEG-Cy3-DSF and LBA-PDA-PEG-Cy3-DSF diluted in culture medium were then added (equivalent to 1μg/mL Cy3) and incubated for 72 h. Then cells were analyzed under a confocal microscope (LSM 700, Carl-Zeiss Inc.).

**b) Cytotoxicity study of LDNP—**SKOV-3 cells were seeded in Corning® Ultra-Low Attachment 96-well plate (20,000 cells/well). After 24 h, each well formed one tumor spheroid. The cells were continued to culture for another 2 days and treated with different DSF, DNP and LDNP with or without $CuCl_2$ (10 μM). The DSF equivalent concentration was 400 nM. PBS and $CuCl_2$ (10 μM) were set as controls. The morphology and diameters of tumor spheroids after the treatments were monitored by light microscopy daily.

### 2.12. Animal model establishment

All animal experiments were conducted in accordance with NIH regulations and approved by the Institutional Animal Care and Use Committee of the University of South Carolina. Ovarian peritoneal metastatic tumor mouse model is established as described in previous study [30]. In brief, luciferase-expressing SKOV-3 cells (SKOV-3 Luc) were suspended in culture medium. Then $1\times10^6$ cells in 200 μL medium were injected intraperitoneally to

female nude mice (8–10 week old, ~20 g, Jackson Laboratories). The weight of mice and the tumor burdens were monitored on a whole body imaging system every week.

### 2.13. Whole body imaging

Tumor growth was monitored by the IVIS Lumina III whole body imaging system (PerkinElmer, Waltham, U.S.A). Briefly, mice were anesthetized by 2% isoflurane, and 100 μL 30 mg/mL D-luciferin was injected intraperitoneally into the tumor-bearing mice. The whole body imaging time was optimized and all mice were imaged using identical system setting. All images were finally processed and the intensity of bioluminescence signal (expressed in radiance) from SKOV3-Luc tumors was quantified by Living Image® software.

### 2.14. In vivo biodistribution

One week after the inoculation of the caner cells, mice were administered with PDA-PEG-Cy3-DSF and LBA-PDA-PEG-Cy3-DSF (Cy3 equal to 10 μg/mL) by *i.p.* injection. Mice were sacrificed and perfused 6 h post-injection. Organs and tumors were collected and imaged *ex vivo* by an IVIS Lumina III whole body imaging system.

### 2.15. Animal treatment

Two weeks after the inoculation of the caner cells, mice were randomly assigned into five groups (n=3) and were given the following five treatments: PBS, DSF, LDNP, DSF/Cu, DNP/Cu and LDNP/Cu. For DSF treatment, DSF was first dissolved in corn oil and injected intraperitoneally. For other treatments, nanoparticle and copper gluconate were first dissolved in PBS respectively, and then mixed just before injection. The final injection volume for all treatments was 250 μL, which includes the equivalent dose of 5 mg/kg for DSF and 0.5 mg/kg for copper gluconate. Mice were given the treatments every week. After three weeks, all mice were sacrificed and the organs and tumors were harvested for further analysis.

### 2.16. Histological Examinations

The fixed organs were embedded in OCT, sectioned into ~10 μm, stained with hematoxylin and eosin (H&E), and analyzed under a light microscope. The histology was performed in a blinded fashion by professional personnel in the University of South Carolina.

### 2.17. Statistical Analysis

Statistical Analysis was performed via the one-way ANOVA using the software SigmaPlot 12.0. (Systat Software Inc., San Jose, CA, USA). The values of $^{*}P < 0.05$ and $^{\#}P < 0.01$ were determined as statistically significant. Data were expressed as means ± standard deviation (SD).

## 3. Results and Discussion

### 3.1. The Synthesis of PDA-PEG-DSF Polymer and Fabrication of DSF Loaded Nanoparticle (DNP)

PDA-PEG polymer was first prepared according to our previous report [25]. The PDA and mPEG in the final PDA-PEG polymer was 1:1. The molecular weight of PDA-PEG polymer was quantified by GPC (Mw: 41.8 kDa; PDI: 1.21). DDTC was then conjugated to the polymer through the thiol-disulfide exchange reaction to obtain the PDA-PEG-DSF polymer (Scheme 2A). The partial replacement of PDA by DDTC in the PDA-PEG polymer was confirmed by $^{1}$H-NMR (Figure 1), evidenced by decreased PDA to PEG ratio in the polymer after the conjugation of DDTC. HPLC was further used to verify the successful conjugation of DDTC to the PDA-PEG polymer via disulfide bonds as proved by the reappearance of DDTC peak after the addition of dithiothreitol (DTT) to cleave the disulfide bond (Figure S2).

β-D-galactose receptor is a surface lectin which is overexpressed in various types of cancer cells, such as liver and ovarian cancers [31]. To endow the polymer with the ovarian cancer targeting effect, lactobionic acid (LBA) was conjugated to the polymer through carbodiimide-mediated coupling reaction (Scheme 2) [29]. The successful conjugation of LBA to the polymer was validated by TNBSA assay through measuring the free amine in the polymer before and after LBA conjugation [32]. A clear decrease of free amine was observed, which revealed that around 54% of LBA was conjugated onto the polymer (10% of PDA). DDTC was then conjugated to LBA-PDA-PEG by replacing residual PDA to yield a functionalized polymer (LBA-PDA-PEG-DSF). Both PDA-PEG-DSF and LBA-PDA-PEG-DSF formed nanoparticles in an aqueous condition (denoted as DNP and LDNP, respectively). DLS results revealed that both DNP and LDNP had sizes around 30 nm and their sizes kept almost the same after the addition of copper chloride (Table 1, Figure S3). TEM images revealed that DNP had a spherical morphology both in the presence and absence of copper ions (Figure 2).

### 3.2. The Release Kinetics of DDTC from DNP

We hypothesized that the DDTC loaded nanoparticle would enter cancer cells through receptor-mediated endocytosis and release DDTC in the cytoplasm, where there is an elevated GSH concentration. To validate this hypothesis, we first investigated the release behavior of DDTC at the presence of 0 and 10 mM GSH to mimic blood circulation and intracellular environments, respectively. No free DDTC was detected after 3 h of incubation in PBS (Figure S4). Furthermore, only negligible amount of DDTC was detected in a serum containing release medium (Figure S4), suggesting that DNP is extremely stable while circulating in the blood. On the contrary, the addition of 10 mM GSH triggered rapid DDTC release (~80% DDTC release within 30 min), indicating that DDTC could be successfully released upon cellular uptake.

### 3.3. Cellular Uptake of LDNP

To validate whether LBA could facilitate DNP entering cancer cells, the cellular uptake behavior of DNP and LDNP was investigated in an ovarian cancer cell line, SKOV-3, which

had been reported overexpressing β-D-galactose receptor [29]. Confocal microscopy revealed that DNP had a low level of cellular uptake (weak red signal), while LDNP exhibited enhanced cellular uptake as evidenced by a strong red signal appeared which inside the cells (Figure 3A). Since the blockage of β-D-galactose receptors by free LBA could significantly inhibit the cellular uptake of LDNP, we ascribe the high uptake of LDNP to the interaction between the LBA and β-D-galactose receptor. Flow cytometry results were consistent with the confocal microscopy finding and further confirmed that LDNP entered cells through the β-D-galactose receptor-mediated endocytosis (Figure 3B).

### 3.4. MTT assay

To investigate whether the enhanced cellular uptake of LDNP could be translated into a better killing effect against cancer cells, MTT assay was employed to evaluate the cytotoxicity of both nanoparticles. SKOV-3 cells were incubated with DSF, DNP and LDNP with or without the presence of 10 μM $CuCl_2$ for 24 h. As shown in Figure 4A, all the treatments had no or just slight toxicity to the SKOV-3 ovarian cancer cells when the copper ion was absent, while the addition of $CuCl_2$ significantly promoted their cytotoxicity. With the addition of $CuCl_2$, both nanoparticles became more potent in killing cancer cells than the free DSF, especially when the drug concentration exceeded 25 nM. Moreover, LDNP with $CuCl_2$ (LDNP/Cu) exhibited the highest cytotoxicity among all treatments. At DSF equivalent to 25 nM, LDNP/Cu had already killed 75% of cancer cells compared to 60% for DNP/Cu and 55% for DSF/Cu. Furthermore, LDNP/Cu eradicated 100% of cancer cells with the DSF concentration of 100 nM. Collectively, the MTT result in combination with confocal and flow cytometry data (Figure 3A and 3B), proved that better cellular uptake of LDNP did translate to higher anticancer efficacy. Moreover, the enhanced anticancer efficacy of LDNP was also observed in liver cancer, colon cancer, breast cancer, as well as drug resistant ovarian cancer cells (Figure S5–9). In contrast to its potent cell killing effect for cancer cells, the combination of LDNP/Cu displayed much lower toxicity for normal liver cells (Figure 4B), suggesting that LDNP/Cu could be a powerful and versatile anticancer tool, while also being safe. Proteasome is a protein complex which regulates many cellular processes involved in proliferation, cell cycle progression, and apoptosis. It have been reported that disulfiram effectively inhibits proteasome activity. Compared with normal cells, proteasome activity is amplified in cancer cells [33], Thus, LDNP/Cu induced apoptosis selectively in cancer cells but not normal cells.

### 3.5. Tumor Spheroid Penetrating Effect of LDNP

It is known that MTT assay in 2-D cell culture has certain limitations in predicting drug efficacy in vivo. For cancer therapy, the anticancer efficacy of a nanoparticle is not only determined by cellular uptake, but also affected by how deep the nanoparticle can penetrate into a solid tumor mass. A multicellular tumor spheroid model resembles many features of solid tumor in vivo, such as high interstitial pressure, poor vascularization, and oxygen/nutrient gradients [34]. Thus, the drug efficacy in a tumor spheroid model can reflect the anticancer efficacy of a nanoparticle in vivo more accurately. Tumor spheroids were formed by culturing SKOV-3 cells in a 96-well plate with ultra-low attachment. Upon the formation of tumor spheroid, the penetration ability of the nanoparticles was explored. DNP and LDNP nanoparticles labeled with Cy3 were incubated with the tumor spheroid for 72 h and

observed under confocal microscopy. The result in Figure 5A revealed that DNP were mainly stalled in the peripheral area of the tumor spheroid, while LDNP penetrated much deeper than DNP, which should consequently result in better tumor eradicating effect.

### 3.6. Tumor Spheroid Disassemble Effect of LDNP

To investigate whether better tumor spheroid penetrating effect could be translated into more potent cell killing effect, the anticancer efficacy of DNP and LDNP were further evaluated in the tumor spheroid model. Tumor spheroids were treated with DSF, DNP and LDNP at DSF equivalent concentration of 400 nM with or without the addition of 10 μM $CuCl_2$ and imaged with a light microscope every 12 h (Figure 5B). Without the addition of copper ions, all tumor spheroids maintained their condensed spherical morphology after 72 h of incubation with different treatments. On the contrary, with the addition of copper ions, LDNP caused complete disintegration of tumor spheroid while DSF and DNP only partially reduced the size of the spheroids. Based on the light microscopy images, the core volume of the tumor spheroids was further calculated and plotted against incubation time. As showed in Figure 5C, LDNP/Cu completely destroyed the tumor spheroid after 48 h of treatment. DSF/Cu reduced 70% of spheroid volume after 60 h, while DNP/Cu only induced 55% volume reduction in the same period of time. We postulate the discrepancy between MTT results and the impact of spheroid volume is due to the fact that DSF penetrates deeper than DNP in a 3-D culture model while penetrating is not needed for a 2-D culture. We believe that the LDNP/Cu shown better penetrative effect is because LDNP can enter cancer cell more easily and cause the disassembly of the tumor mass, which subsequently create the space for nanoparticle to diffuse through. All these tumor spheroid results (Figure 5A–C) confirmed that the DSF loaded nanoparticle was effective in killing cancer cells and the targeting ligand LBA did enhance its anticancer efficacy, making it worthwhile to be further evaluated in vivo.

### 3.7. In Vivo Biodistribution of LDNP

Intraperitoneal metastasis is commonly observed clinically in late-stage ovarian cancer patients, which has a 5-year survival rate less than 40% [35]. To investigate the anticancer efficacy of LDNP nanoparticle in vivo, a clinically relevant peritoneal metastatic ovarian tumor model was established by i.p. injection of luciferase-expression SKOV-3 cells (SKOV-3-Luc) into nude mice according to previous reports [36]. Since the bioluminescence intensity is proportional to cell population in a tumor (Figure S10), for this tumor model, the tumor size can be easily monitored by measuring the bioluminescence intensity of the mice. The biodistribution of the Cy3 labeled DNP and LDNP nanoparticles were studied with the help of an IVIS imaging system. Both DNP and LDNP nanoparticles were found localized mainly in liver, lungs, kidney and tumors (left in Figure 6A). Both nanoparticles exhibited an enhanced retention in tumors as the brightest Cy3 signal was colocalized with the luminescence signal of the tumor (right in Figure 6B). The high level of accumulation in the tumor tissue is probably due to the so called “EPR effect” as a result of leaking blood capillaries and deficiency of lymphatic system in the tumor [37]. Compared with DNP, LDNP accumulated more in kidney while less in liver.

### 3.8. Tumor Growth Inhibitory Effect of LDNP

The anticancer efficacy of the nanoparticles were further investigated in an peritoneal metastatic ovarian tumor model by i.p. administeration of DSF, DNP and LDNP with or without the addition of copper ions. Copper gluconate, an FDA approved dietary supplement, was adopted as a copper source because it has been clinically used in combination with DSF in several trials for cancer therapy. The luminescence of the mice was recorded weekly. As shown in Figure 7A, a dramatic increase of the luminescence was observed in control mice three weeks after initial treatment, indicating the rapid growth of tumor in the mice. Contrast to the control group, DSF/Cu and DNP/Cu treated groups showed weaker luminescence, suggesting that DSF/Cu and DNP/Cu could effectively retard the progression of tumor cells.

The LDNP nanoparticle coupled with copper ions showed the best efficacy in impeding tumor growth as only a faint signal was observed. To be noted, LDNP without copper also exhibited low luminescence probably due to the elevated copper level in tumor mass serving as a copper source [17], thus resulting in plausible anticancer effect. The luminescence intensities (radiance) of all treatments were summarized in Figure 7B, which also confirmed that both nanoparticles coupled with copper ions could effectively inhibit the progression of tumor.

To examine the detailed anticancer efficacy of the above treatments, mice were sacrificed 3 weeks post treatment. Many tumors were found in the abdominal cavities of the control and DSF/Cu treated mice, including tissue beneath the skin, mesentery and the external surface of intestines (Figure S11). On the contrary, much fewer tumors were found in both nanoparticles treated mice. Consistent with bioluminescence images, nanoparticles, especially the targeted one, resulted in significant tumor burden reduction. LDNP/Cu reduced the tumor weight by 86% and tumor number by 83% (Figure 7C and 7D) as compared with control group. We postulate the reason that DSF/Cu treatment didn’t exhibit significant tumor growth inhibitory effect was due to the crystallization of DSF and Cu at high concentration. Although tumor tissue has higher copper concentration than normal tissue, however, that amount of copper in tumor tissue itself is not sufficient to make the LDNP effective enough to inhibit the growth of the tumor, as evidenced by Figure 7C and 7D. Therefore, we think the introduction of additional copper is necessary to achieve effective tumor growth inhibitory effect.

### 3.9. Systemic toxicity of LDNP

The systemic toxicity of the nanoparticles were evaluated by monitoring the body weight of the mice and liver histology. The body weight did not significantly change in all treatment groups (Figure 8A). In addittion, the histological examination of liver tissues did not find any noticeable damage or difference among all liver tissue sections (Figure 8B). According to literature [38], daily dose of 30–60 mg for 3 years can cause cirrhosis. Since the dose we used is 0.5 mg/kg, which is corresponding to 35 mg per weekly treatment (assuming the patient has a weight of 70 kg), which is far lower than the dose given in the ref. In addition, for cancer treatment, it is not necessary to treat the patient for long period of time if the

treatment is effective. Altogether, the in vivo data indicate that the LDNP/Cu nanoparticle could be an effective and safe tool for the treatment of advanced ovarian cancer.

## 4. Conclusion

In summary, disulfiram metabolite, DDTC, conjugated nanoparticles were fabricated and modified with targeting ligands (LBA) to repurpose DSF for cancer therapy. The nanoparticle can efficiently enter cancer cells through β-D-galactose receptor mediated endocytosis. Upon cellular uptake, due to the intracellular high GSH level, the LDNP nanoparticle degrades and releases DDTC, which subsequently forms active complex with copper and kills a broad spectrum of cancer cells while not affecting normal cells. Furthermore, LDNP showed stronger penetrating and destructive capacity in a tumor spheroid model. In vivo study carried out in a clinically relevant peritoneal metastatic ovarian tumor model revealed that LDNP/Cu exhibits stronger efficacy in inhibiting the progression of metastatic ovarian cancer than the regimen used in clinical trials, while not inducing side effects.

## Supplementary Material

Refer to Web version on PubMed Central for supplementary material.

## Acknowledgments

The authors want to thank National Institutes of Health (1R15CA188847-01A1 and 1R01AG054839-01A1) for financial support of the research.

## References

1. Hald J, Jacobsen E. A drug sensitizing the organism to ethyl alcohol. Lancet. 1948; 2(6539):1001–4. [PubMed: 18103475]
2. Cvek B. Nonprofit drugs as the salvation of the world's healthcare systems: the case of Antabuse (disulfiram). Drug Discovery Today. 2012; 17(9–10):409–412. [PubMed: 22192884]
3. Cvek B, Dvorak Z. The value of proteasome inhibition in cancer. Drug Discovery Today. 2008; 13(15–16):716–722. [PubMed: 18579431]
4. Liu P, Brown S, Goktug T, Channathodiyil P, Kannappan V, Hugnot JP, Guichet PO, Bian X, Armesilla AL, Darling JL, Wang W. Cytotoxic effect of disulfiram/copper on human glioblastoma cell lines and ALDH-positive cancer-stem-like cells. Brit J Cancer. 2012; 107(9):1488–1497. [PubMed: 23033007]
5. Chen D, Cui QZC, Yang HJ, Dou QP. Disulfiram, a clinically used anti-alcoholism drug and copper-binding agent, induces apoptotic cell death in breast cancer cultures and xenografts via inhibition of the proteasome activity. Cancer Research. 2006; 66(21):10425–10433. [PubMed: 17079463]
6. Brar SS, Grigg C, Wilson KS, Holder WD, Dreau D, Austin C, Foster M, Ghio AJ, Whorton AR, Stowell GW, Whittall LB, Whittle RR, White DP, Kennedy TP. Disulfiram inhibits activating transcription factor/cyclic AMP-responsive element binding protein and human melanoma growth in a metal-dependent manner in vitro, in mice and in a patient with metastatic disease. Molecular Cancer Therapeutics. 2004; 3(9):1049–1060. [PubMed: 15367699]
7. Shiah SG, Kao YR, Wu FYH, Wu CW. Inhibition of invasion and angiogenesis by zinc-chelating agent disulfiram. Molecular Pharmacology. 2003; 64(5):1076–1084. [PubMed: 14573756]
8. Duan XP, Xiao JS, Yin Q, Zhang ZW, Yu HJ, Mao SR, Li YP. Smart pH-Sensitive and Temporal-Controlled Polymeric Micelles for Effective Combination Therapy of Doxorubicin and Disulfiram. ACS nano. 2013; 7(7):5858–5869. [PubMed: 23734880]

9. Loo TW, Clarke DM. Blockage of drug resistance in vitro by disulfiram, a drug used to treat alcoholism. Journal of the National Cancer Institute. 2000; 92(11):898–902. [PubMed: 10841824]
10. Loo TW, Bartlett MC, Clarke DM. Disulfiram metabolites permanently inactivate the human multidrug resistance P-glycoprotein. Molecular Pharmaceutics. 2004; 1(6):426–433. [PubMed: 16028354]
11. Lopez-Lazaro M. Dual role of hydrogen peroxide in cancer: Possible relevance to cancer chemoprevention and therapy. Cancer Letters. 2007; 252(1):1–8. [PubMed: 17150302]
12. Wang WG, McLeod HL, Cassidy J. Disulfiram-mediated inhibition of NF-kappa B activity enhances cytotoxicity of 5-fluorouracil in human colorectal cancer cell lines. International Journal of Cancer. 2003; 104(4):504–511. [PubMed: 12584750]
13. Xu B, Shi PC, Fombon IS, Zhang YY, Huang F, Wang WG, Zhou SY. Disulfiram/copper complex activated JNK/c-jun pathway and sensitized cytotoxicity of doxorubicin in doxorubicin resistant leukemia HL60 cells. Blood Cell Mol Dis. 2011; 47(4):264–269.
14. Zhang L, Tian B, Li Y, Lei T, Meng J, Yang L, Zhang Y, Chen F, Zhang HT, Xu H, Zhang Y, Tang X. A Copper-Mediated Disulfiram-Loaded pH-Triggered PEG-Shedding TAT Peptide-Modified Lipid Nanocapsules for Use in Tumor Therapy. ACS applied materials & interfaces. 2015; 7(45): 25147–25161. [PubMed: 26501354]
15. Koppaka V, Thompson DC, Chen Y, Ellermann M, Nicolaou KC, Juvonen RO, Petersen D, Deitrich RA, Hurley TD, Vasiliou V. Aldehyde Dehydrogenase Inhibitors: a Comprehensive Review of the Pharmacology, Mechanism of Action, Substrate Specificity, and Clinical Application. Pharmacol Rev. 2012; 64(3):520–539. [PubMed: 22544865]
16. Schmitt SM, Frezza M, Dou QP. New applications of old metal-binding drugs in the treatment of human cancer. Frontiers in bioscience. 2012; 4:375–91.
17. Gupte A, Mumper RJ. Elevated copper and oxidative stress in cancer cells as a target for cancer treatment. Cancer treatment reviews. 2009; 35(1):32–46. [PubMed: 18774652]
18. Wang WG, Darling JL. How could a drug used to treat alcoholism also be effective against glioblastoma? Expert Rev Anticanc. 2013; 13(3):239–241.
19. Nagai N, Yoshioka C, Mano Y, Tnabe W, Ito Y, Okamoto N, Shimomura Y. A nanoparticle formulation of disulfiram prolongs corneal residence time of the drug and reduces intraocular pressure. Experimental eye research. 2015; 132:115–23. [PubMed: 25633346]
20. Hoda M, Sufi SA, Shakya G, Kumar KM, Rajagopalan R. Influence of stabilizers on the production of disulfiram-loaded poly(lactic-co-glycolic acid) nanoparticles and their anticancer potential. Ther Deliv. 2015; 6(1):17–25. [PubMed: 25565438]
21. Fasehee H, Zarrinrad G, Tavangar SM, Ghaffari SH, Faghihi S. The inhibitory effect of disulfiram encapsulated PLGA NPs on tumor growth: Different administration routes. Materials science & engineering. C, Materials for biological applications. 2016; 63:587–95. [PubMed: 27040254]
22. Fasehee H, Dinarvand R, Ghavamzadeh A, Esfandyari-Manesh M, Moradian H, Faghihi S, Ghaffari SH. Delivery of disulfiram into breast cancer cells using folate-receptor-targeted PLGA-PEG nanoparticles: in vitro and in vivo investigations. Journal of nanobiotechnology. 2016; 14:32. [PubMed: 27102110]
23. Liu P, Wang ZP, Brown S, Kannappan V, Tawari PE, Jiang WG, Irache JM, Tang JZ, Britland S, Armesilla AL, Darling JL, Tang X, Wang WG. Liposome encapsulated Disulfiram inhibits NF kappa B pathway and targets breast cancer stem cells in vitro and in vivo. Oncotarget. 2014; 5(17): 7471–7485. [PubMed: 25277186]
24. Duan XP, Xiao JS, Yin Q, Zhang ZW, Yu HJ, Mao SR, Li YP. Multi-targeted inhibition of tumor growth and lung metastasis by redox-sensitive shell crosslinked micelles loading disulfiram. Nanotechnology. 2014; 25(12)
25. Bahadur RKC, Xu P. Multicompartment Intracellular Self-Expanding Nanogel for Targeted Delivery of Drug Cocktail. Advanced Materials. 2012; 24(48):6479–6483. [PubMed: 23001909]
26. Remant BK, Chandrashekaran V, Cheng B, Chen H, Pena MM, Zhang J, Montgomery J, Xu P. Redox potential ultrasensitive nanoparticle for the targeted delivery of camptothecin to HER2-positive cancer cells. Mol Pharm. 2014; 11(6):1897–905. [PubMed: 24779647]
27. He H, Altomare D, Ozer U, Xu H, Creek K, Chen H, Xu P. Cancer cell-selective killing polymer/copper combination. Biomaterials Science. 2016

28. Gunn AJ, Hama Y, Koyama Y, Kohn EC, Choyke PL, Kobayashi H. Targeted optical fluorescence imaging of human ovarian adenocarcinoma using a galactosyl serum albumin-conjugated fluorophore. Cancer science. 2007; 98(11):1727–1733. [PubMed: 17784874]
29. Wu F, Wuensch SA, Azadniv M, Ebrahimkhani MR, Crispe IN. Galactosylated LDL Nanoparticles: A Novel Targeting Delivery System To Deliver Antigen to Macrophages and Enhance Antigen Specific T Cell Responses. Molecular Pharmaceutics. 2009; 6(5):1506–1517. [PubMed: 19637876]
30. Cho EJ, Sun B, Doh KO, Wilson EM, Torregrosa-Allen S, Elzey BD, Yeo Y. Intraperitoneal delivery of platinum with in-situ crosslinkable hyaluronic acid gel for local therapy of ovarian cancer. Biomaterials. 2015; 37:312–319. [PubMed: 25453960]
31. Gunn AJ, Hama Y, Koyama Y, Kohn EC, Choyke PL, Kobayashi H. Targeted optical fluorescence imaging of human ovarian adenocarcinoma using a galactosyl serum albumin-conjugated fluorophore. Cancer science. 2007; 98(11):1727–33. [PubMed: 17784874]
32. He H, Citron AW, Nguyen T, Nieminen AL, Xu P. Triple-responsive expansile nanogel for tumor and mitochondria targeted photosensitizer delivery. Biomaterials. 2014; 35(35):9546–9553. [PubMed: 25154666]
33. Kumatori A, Tanaka K, Inamura N, Sone S, Ogura T, Matsumoto T, Tachikawa T, Shin S, Ichihara A. Abnormally high expression of proteasomes in human leukemic cells. Proc Natl Acad Sci U S A. 1990; 87(18):7071–5. [PubMed: 2205851]
34. Zanoni M, Piccinini F, Arienti C, Zamagni A, Santi S, Polico R, Bevilacqua A, Tesei A. 3D tumor spheroid models for in vitro therapeutic screening: a systematic approach to enhance the biological relevance of data obtained. Scientific reports. 2016; 6
35. Satpathy M, Cao L, Pincheira R, Emerson R, Bigsby R, Nakshatri H, Matei D. Enhanced peritoneal ovarian tumor dissemination by tissue transglutaminase. Cancer Res. 2007; 67(15): 7194–202. [PubMed: 17671187]
36. Cho EJ, Sun B, Doh KO, Wilson EM, Torregrosa-Allen S, Elzey BD, Yeo Y. Intraperitoneal delivery of platinum with in-situ crosslinkable hyaluronic acid gel for local therapy of ovarian cancer. Biomaterials. 2015; 37:312–319. [PubMed: 25453960]
37. Cabral H, Kataoka K. Progress of drug-loaded polymeric micelles into clinical studies. Journal of Controlled Release. 2014; 190:465–476. [PubMed: 24993430]
38. O'Donohue J, Reid M, Varghese A, Portmann B, Williams R. A case of adult chronic copper self-intoxication resulting in cirrhosis. Eur J Med Res. 1999; 4(6):252. [PubMed: 10383882]

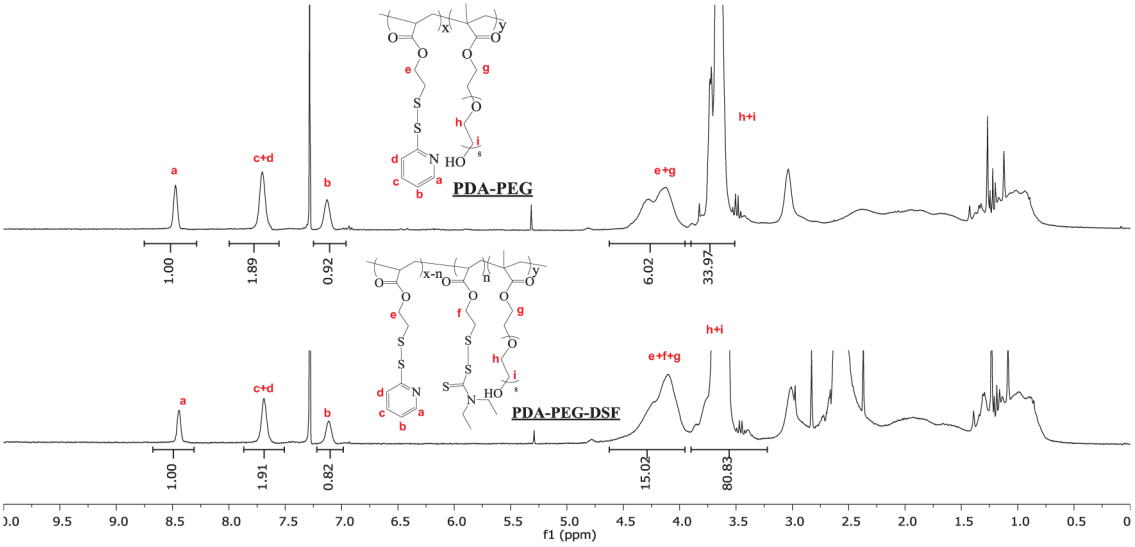


**Figure 1.**

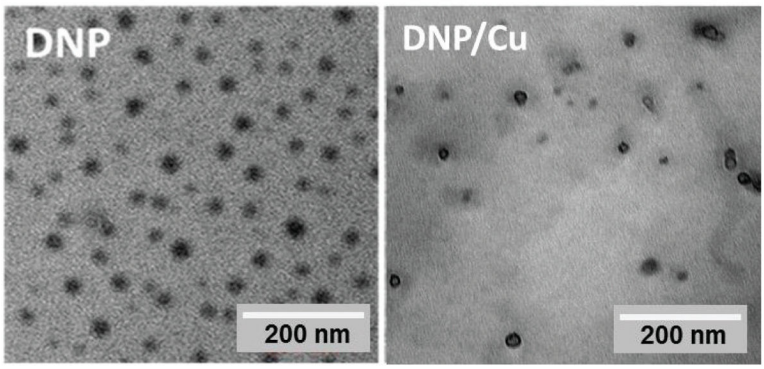


**Figure 2.**

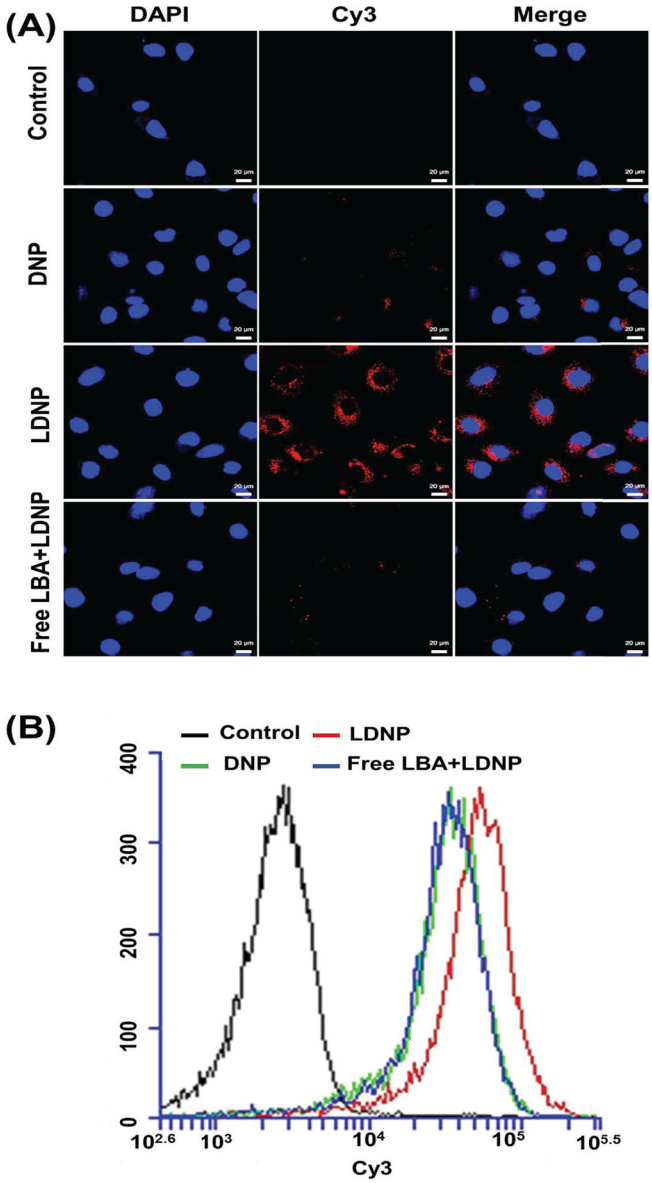


**Figure 3.**

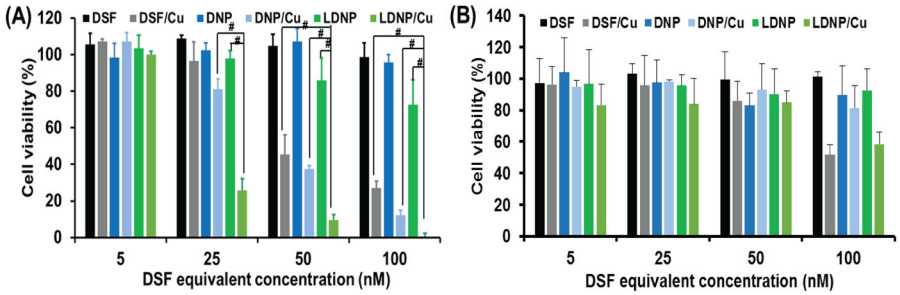


**Figure 4.**

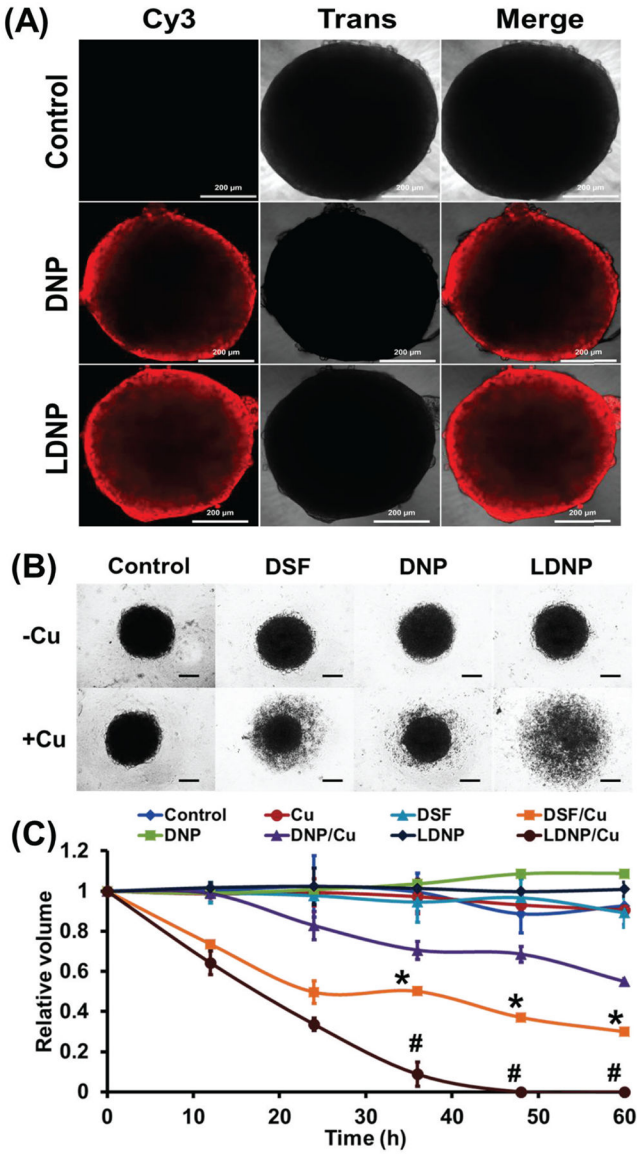


**Figure 5.**

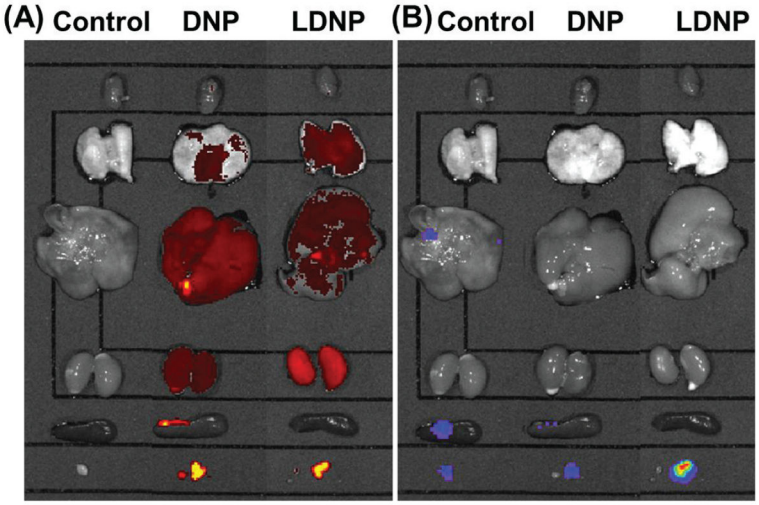


**Figure 6.**

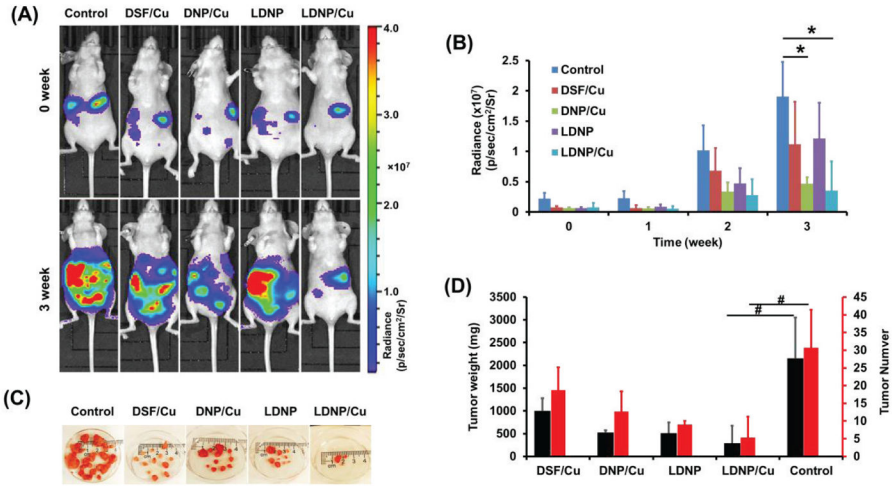


**Figure 7.**

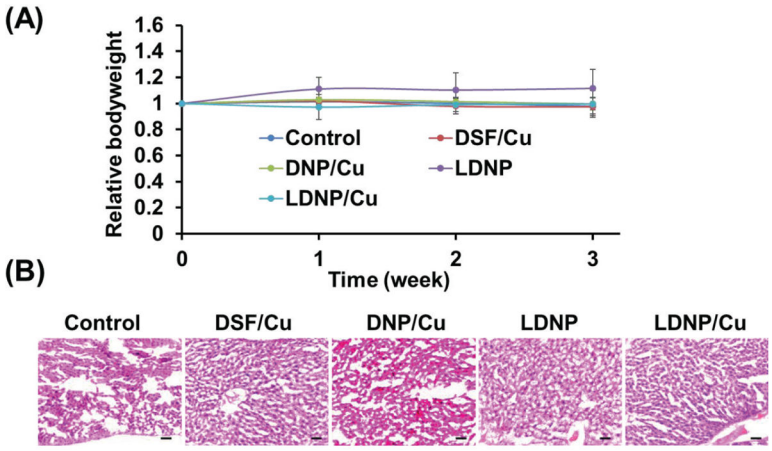


**Figure 8.**

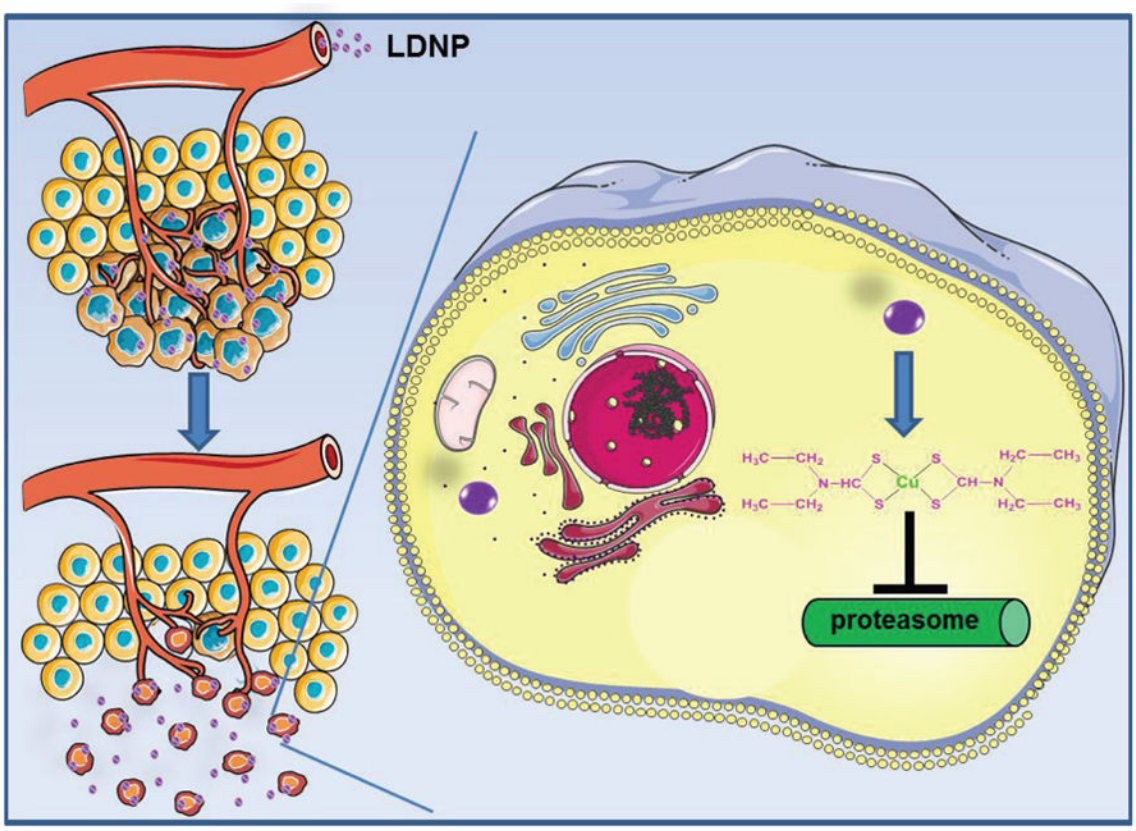


**Figure 9.**

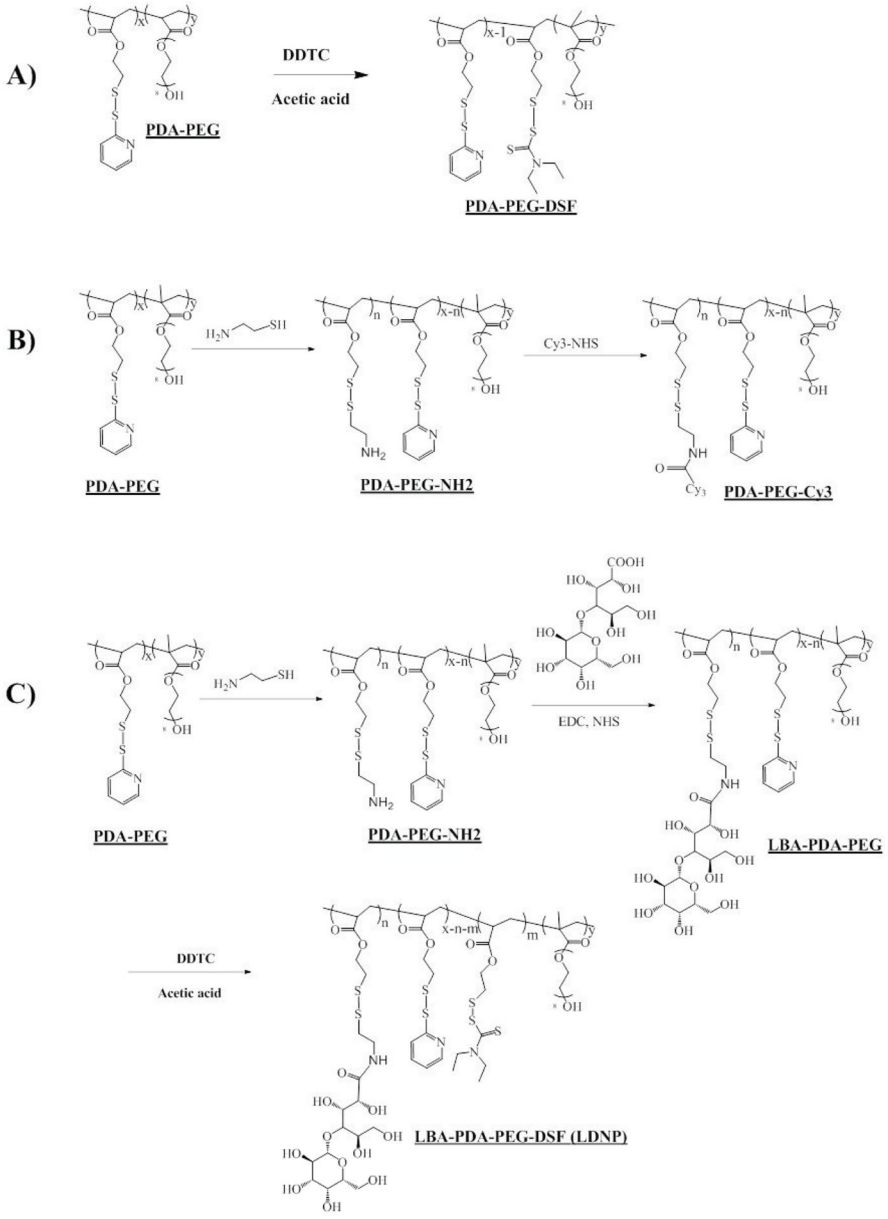


**Figure 10.**

**Table 1**

| | DNP Size (nm) | PDI | LDNP Size (nm) | PDI |
|---|---|---|---|---|
| −Cu | 35.17±0.35 | 0.51±0.038 | 30.05±0.42 | 0.415±0.013 |
| +Cu | 36.1±0.62 | 0.489±0.0006 | 29.48±0.78 | 0.395±0.013 |